IOPscience iopscience.iop.org

Home Search Collections Journals About Contact us My IOPscience

In situ thermal evolution of B–B pairs in crystalline Si: a spectroscopic high resolution x-ray diffraction study

This article has been downloaded from IOPscience. Please scroll down to see the full text article.

2008 J. Phys.: Condens. Matter 20 175215

(http://iopscience.iop.org/0953-8984/20/17/175215)

View the table of contents for this issue, or go to the journal homepage for more

Download details:
IP Address: 129.252.86.83
The article was downloaded on 29/05/2010 at 11:38

Please note that terms and conditions apply.

J. Phys.: Condens. Matter **20** (2008) 175215 (4pp) doi:10.1088/0953-8984/20/17/175215

In situ thermal evolution of B–B pairs in crystalline Si: a spectroscopic high resolution x-ray diffraction study

G Bisognin[1], D De Salvador[1], E Napolitani[1], A Carnera[1], E Bruno[2], S Mirabella[2], A M Piro[2], L Romano[2] and M G Grimaldi[2]

[1] MATIS CNR-INFM and Dipartimento di Fisica, Università di Padova, via F Marzolo 8, 35131 Padova, Italy
[2] MATIS CNR-INFM and Dipartimento di Fisica ed Astronomia, Università di Catania, via S Sofia 64, 95123 Catania, Italy

E-mail: bisognin@padova.infm.it

Received 11 February 2008, in final form 11 March 2008
Published 7 April 2008
Online at stacks.iop.org/JPhysCM/20/175215

Abstract
The lattice strain induced by the thermal evolution of B–B pairs formed in a $Si_{1-x}B_x$/Si layer as a consequence of He irradiation has been studied *in situ* in an N_2 atmosphere, by using a high resolution x-ray diffractometer equipped with a hot stage sample holder. The collection of repeated rocking curves during a linear temperature (T) ramp allowed monitoring of the effects of the B–B pair thermal evolution on the epilayer lattice parameter a (and equally its strain) during the whole of the annealing from room T up to their complete dissolution (883 °C). By analysing the evolution of $a(T)$ we extracted detailed information about the kinetics of B–B pair evolution. This allowed us to determine an experimental description of the B–B pair dissolution path in good agreement with recent *ab initio* calculations.

1. Introduction

The continuing need to shrink the device dimensions imposed by the International Technology Road Map drives the technological and scientific community toward an extraordinarily detailed study of one of the main problems connected with B ion implantation in Si: B clustering (BC) [1]. Its comprehension, despite the detrimental action of BC on B electrical activity, is still an open and key point to overcome in order to progress in the realization of ultra-shallow junctions. In fact, information coming from both experimental [2–5] and theoretical [6–9] methods did not produce a homogeneous picture of the phenomenon. However, in order to understand BC, attention must be focused on the very small BC precursors (BC-Ps). From an inverse modelling approach with experimental data collected at high temperature, they were predicted to already form during B implantation or at the very early stage of the annealing [10]. The information gap between B clusters and BC-Ps is probably due to the experimental difficulty in their detection.

Recently, it was observed that the stable B–B pair (B_2I) is the defect formed already at room temperature (RT) as a consequence of the B displacement from substitutional sites induced by ion irradiation with MeV H or He beams [11–14]. These B_2I pairs could operate as the seeds of large BCs just during the annealing ramp or in the implantation process itself.

In this work, an *in situ* spectroscopic approach to high resolution x-ray diffraction (HRXRD) [15] is exploited to investigate the B–B complex under thermal annealing in the RT–883 °C range, i.e. until its complete dissolution occurs. The choice of HRXRD as the main experimental technique is motivated by the fact that these B–B complexes are very small and so inaccessible with the methodologies classically exploited to study defect evolution in semiconductors (i.e. transmission electron microscopy). In contrast, HRXRD does not suffer from this limitation [15].

2. Experimental details

A 430 nm thick $Si_{0.9984}B_{0.0016}$ layer was grown by molecular beam epitaxy (MBE) on an n-type Si(001) substrate and then irradiated by a 300 keV, 2.4×10^{15} He cm^{-2} total fluence at random incidence (no voids are formed for this low He

 © 2008 IOP Publishing Ltd Printed in the UK

irradiation dose [16]). For further details about both growth and processing see [17]. Nuclear reaction analysis (NRA), both in random and in channelling configurations, has been performed using the ^{11}B(p, alpha)^{8}Be nuclear reaction with a 650 keV proton beam and detecting emitted alpha particles. For more details see [12]. HRXRD spectra were collected with a Philips MRD X-Pert PRO™ diffractometer in the triple-axis configuration. After RT HRXRD measurements on the sample before and after He irradiation, we used a parabolic mirror and an Anton Paar DHS 900 hot stage to collect fast ω–2θ scans (rocking curves (RCs)) *in situ* with an N_2 atmosphere during a linear annealing ramp (the temperature increased by 3 °C every 8 min). The effective temperature at the sample was checked by measuring the Si substrate dilatation, finding that the sample follows the holder T within ±(3–4) °C.

3. Results and discussion

NRA channelling measurements have been performed on the as-grown (AG) MBE sample and after its He irradiation (AI). Angular scans confirmed that all pristine substitutional B (B_s) (∼95%) was converted into B–B pairs. Their formation process can be summarized in the following way [11]: (i) Si self-interstitials (Is) generated by the He beam are trapped by B_s; (ii) the mobile B–I couple migrates at room temperature; (iii) a stable, not mobile and energetically favoured B complex (B–B pair) is formed. The first step is energetically favoured, since the B–I couple formation has a binding energy of 0.90 eV [18], while the room temperature migration of B has been recently evidenced [19]. Finally, several molecular dynamics simulations and first-principles studies of the energetics [18, 20, 21] have indicated that a B–B pair oriented along the ⟨100⟩ axis is the lowest energy configuration.

Finally, we neglect vacancy contributions on the basis of the results of [22], in which it is reported that vacancies anneal very quickly for T values below RT.

For all these reasons we can say that, after He irradiation, the B–B pairs are our starting point.

This B clustering is detectable also in figure 1, in which the RCs of the sample before (open symbols) and after (dash–dotted line) He irradiation are shown.

There are two main changes induced by He irradiation in the HRXRD spectrum: (i) the strong shift of the B-doped layer Bragg peak toward lower angles (B–B pairs reduce by about 40% [17] of the original negative strain of B_s [23]) and (ii) the appearance of a shoulder at negative angles aside the Si Bragg peak, due to the deep (∼1.3 μm) positively strained damaged region induced by the He implant [17]. The shift of the B-doped epilayer Bragg peak is the more important He irradiation effect, since it confirms that all B atoms are involved in the B–B pair formation (see also the negative strain profiles of the AG and AI samples in [17]) and that the epilayer Bragg peak position is governed only by B–B complex changes. Moreover, the annealing effect on both the epilayer Bragg peak and the shoulder at negative angles is visible on observing the RCs collected at 316 and 500 °C, respectively (see the continuous thin line and the dashed line of figure 1):

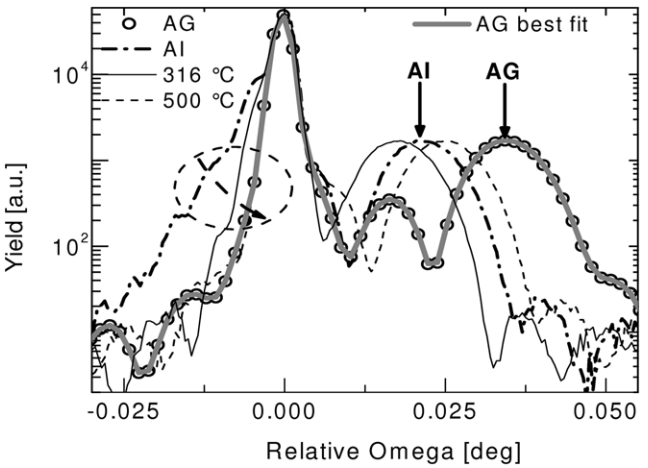

Figure 1. HRXRD RCs of the AG (open circles) and AI sample (dash–dotted line). Continuous thin and dashed lines refer to AI +316 and +500 °C, respectively. The very thick grey line is the simulation of the AI RC. The dashed–circled arrow indicates the lowering of the compressive shoulder extent, corresponding to damage dissolution.

while the epilayer Bragg peak spans lower (316 °C) and higher (500 °C) values with respect to the AI angular position, the compressive shoulder monotonically decreases.

The fact that interference fringes are present and their period, which is related to the negative strained region thickness, remains the same until B–B pairs are dissolved, suggests pseudomorphicity of the epilayer, as also verified by reciprocal space maps (RSMs) recorded around the (004) and (224) reflections (not reported here). RSMs were recorded also after the higher T annealing undergone by the sample (883 °C). Also in this case the B-doped epilayer was found to be pseudomorphic to the substrate. This fundamental fact allows one to extract the relaxed lattice parameter a_{rel} of the B-doped layer (i.e. the lattice parameter of the epilayer once the epitaxial constraint was removed) by using the elasticity theory and just only one (004) RC. Moreover, the a_{rel} variation of the B-doped epilayer shown in the following is not due to thermal strain, as verified by measuring both AG and AI samples before and after their cooling from 800 °C down to RT, finding no difference between RCs collected at these two T values (not reported here).

In figure 2(a) the evolution of a_{rel} as a function of the annealing T is shown (circles). It is clear that a_{rel} is not a simple and monotonic function of T and its behaviour can be divided into four main regimes (see figure 2(a)), which alternate a decrease (regimes (A) and (C)) with an increase (regimes (B) and (D)) of $a_{rel}(T)$. Qualitatively, this complex trend reveals that B–B pairs inside the layer undergo many transformation steps at different T values since, quite reasonably, each of them has to overcome a particular energy barrier E to occur. In order to extract quantitative information from this trend, it is useful to consider the derivative of $a_{rel}(T)$ with respect to T, i.e. a sort of 'strain evolution speed' plot that is shown in figure 2(b).

This plot evidences five main peaks (minima and maxima, marked by arrows) and the related T (see the second column

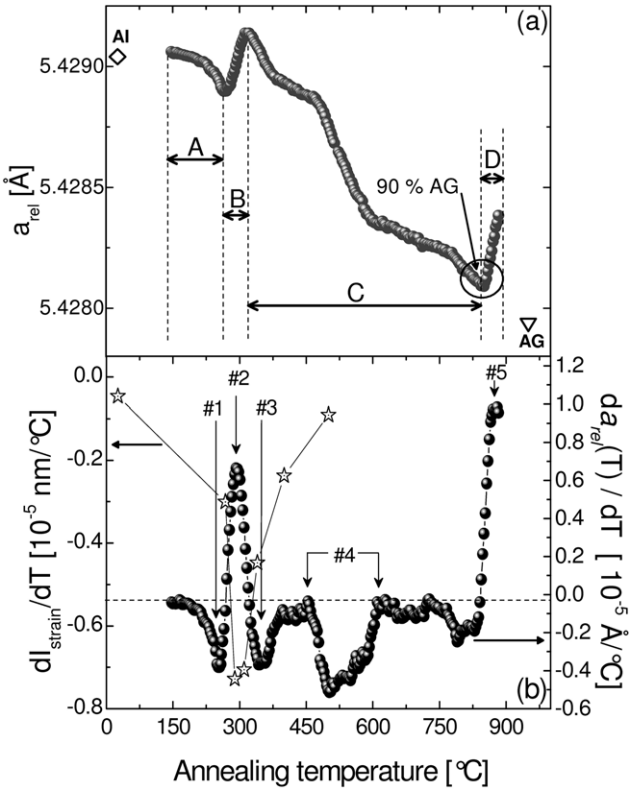

Figure 2. (a) B-doped relaxed lattice parameter as a function of the annealing temperature. (b) Derivative of $I_{\mathrm{strain}}(T)$ and of $a_{\mathrm{rel}}(T)$ with respect to T (stars and circles, respectively) as a function of the annealing temperature.

of table 1), indicating the presence of as many main strain instabilities related to transformation processes in the B–B pair evolution.

In order to extract the E values associated with each strain instability, we based our reasoning on the idea that B–B pairs, thanks to the annealing, evolve into different complexes. Moreover, each particular complex present in the lattice gives a particular strain (i.e. the a_{rel} value) proportional to its abundance. When the complex dissolves, the related strain is released. The complex dissolution happens by overcoming the energy barrier E. Under this hypothesis, it is possible to write the following equation that describes the time evolution of a_{rel} due to the complex dissolution [15]:

$$\frac{\mathrm{d}a_{\mathrm{rel}}(t)}{\mathrm{d}t} = (a_{\mathrm{rel}}(t) - a_{\mathrm{end}})\nu_0\,\mathrm{e}^{-\left(\frac{E}{Krt}\right)}, \qquad (1)$$

where $a_{\mathrm{rel}}(t)$ is the epilayer relaxed lattice parameter as a function of the time, a_{end} is the value assumed by $a_{\mathrm{rel}}(t)$ once the process saturates, ν_0 is the attempt frequency of the process, r is the rate of the ramp (and therefore $rt = T$), K the Boltzmann constant and E represents its activation energy.

It is quite intuitive that $\frac{\mathrm{d}a_{\mathrm{rel}}(T)}{\mathrm{d}T}$ regulated by equation (1) has a bell shape. In fact, by increasing T, the transformation process first raises its speed, because of the increasing of the term $\nu_0\,\mathrm{e}^{-\left(\frac{E}{Krt}\right)}$ in equation (1). For higher T the speed decreases, since $a_{\mathrm{rel}}(t)$ progressively approaches a_{end}. By some mathematical elaborations it is possible to demonstrate that

Table 1. Schematic summary of the instability number (column No 1), and of their thermal location (column No 2), and the comparison between experimental and theoretical values for the dissolution barriers E connected to the instabilities themselves (columns No 3 and No 4, respectively). The last column describes from a microscopic point of view the processes associated with each strain instability.

Process	T_{peak} (°C)	E (eV)	E_{th} (eV)	Event
1	253	1.7	—	Lattice arrangement
2	293	1.8	—	Is flux
3	352	2.0	(2.0–2.3) [6, 7]	$B_2I_2 \rightarrow B_2I$
4	475–594	2.4–2.9	(1.8–2.7) [6, 7]	$B_2I \rightarrow B$
5	876	3.8	(3.12–3.75) [26]	B diffusion

the maximum value of $\frac{\mathrm{d}a_{\mathrm{rel}}(T)}{\mathrm{d}T}$ is related to E according to the implicit relation [15]

$$\frac{Er}{KT_{\mathrm{peak}}^2} - \nu_0\,\mathrm{e}^{-\left(\frac{E}{KT_{\mathrm{peak}}}\right)} = 0, \qquad (2)$$

where T_{peak} is the temperature at which the process reaches its maximum speed. Equation (2) can be numerically managed and it allows us to find E once T_{peak} is measured (see the third column of table 1). For the calculation we assumed $\nu_0 = 10^{13}$ Hz, i.e. the typical Si phonon frequency, supposing that the dissolution process is simply thermally activated and not mediated by interaction with other species.

Once the five E values have been derived (see table 1), we try to understand the physical origin of the corresponding strain instabilities. First of all we focus on the two maxima No 2 and No 5 in figure 2(b). Maximum No 2 originates in the region in which $a_{\mathrm{rel}}(T)$ reverses its trend, i.e. $a_{\mathrm{rel}}(T)$ raises its value for the first time. This is due to the Si self-interstitials (Is) released by the above mentioned damaged zone produced by the He implantation [24] and revealed by HRXRD [17]. This is confirmed by the fact that the Is positive strain, shown by the compressive shoulder beside the Si Bragg peak of the AI sample RC (dash–dotted line of figure 1), lowers its extent by raising T (see for example the RC collected at 316 °C (continuous thin line of figure 1)). RC simulations allow us to quantitatively extract the strain integral (I_{strain}) of the damaged region as a function of T. By calculating $\mathrm{d}I_{\mathrm{strain}}(T)/\mathrm{d}T$ (see the stars in figure 2(b)) and observing that a minimum is present at exactly the same T as the maximum No 2, we can very reasonably assert that the damage dissolution is the cause of the strain instability No 2. In fact, Is migrate toward the B-doped region, interacting with the B–B clusters. This process leads to an a_{rel} increase, in agreement with the results found in [25], where it was demonstrated that large and complex B clusters characterized by positive strain can be formed if B_s interacts with a high Is supersaturation. However the Is reservoir supplied by the He implant damage is limited and so the exhaustion of the I_{strain}, together with the increase of T, is accompanied by a new inversion of $a_{\mathrm{rel}}(T)$ toward the AG value.

As regards the instability No 5, the strain profile (not shown) extracted by simulating the RC taken at 883 °C reveals (i) that the mean strain value in the B-doped layer is lower with

respect to that found in the AG case and (ii) more importantly, a pronounced negative strain tail is present between 430 and 650 nm, i.e. beyond the original $Si_{0.9984}B_{0.0016}$/Si interface. After checking that the I_{strain} (i.e. the B dose) at 883 °C is the same as that of I_{strain} (RT), we can state that these two features are the fingerprint of B diffusion. This fact is supported also by the comparison between E_5 and the literature B diffusion activation energy (E_{DB}), which spans 3.12–3.75 eV [26].

The interpretation of minima Nos 3, 4 and 1 is not as easy as for the previous considered maxima. A comparison with theoretical predictions, as will be see below, gives us some suggestions for completing the identification of the B–B pair evolution steps. Channelling studies [11–14] demonstrated that, even if the presence of other types of clusters cannot be excluded (in particular $B_2I_{x>1}$), the predominant defect formed after He irradiation is the B_2I pair. Very reasonably, at relatively low T, Is released by lattice damage interact with a fraction of B_2I, leading to the formation of B_2I_2 complexes. Then B_2I_2 and B_2I complexes dissolve, giving rise to the strain instabilities No 3 and No 4, respectively, with E_3 and E_4 values very close to *ab initio* theoretical predictions [6, 7] (see table 1). In particular for minimum No 4, since its width is probably the convolution of different instabilities thermally located very close to each other. However, at the end of instability No 4, $a_{rel} \neq a_{rel-AG}$. To investigate in more detail both minimum No 3 and minimum No 4 we performed NRA channelling analyses for samples for which the linear rump was interrupted at $T = 400$ and 600 °C, i.e. when the third and fourth strain instability saturations, respectively, were achieved. While at $T = 400$ °C all B turns out to be out of the site, in agreement with the $B_2I_2 \rightarrow B_2I$ reaction, after the exhaustion of instability No 4 the minimum channelling yield lowers, indicating that only part of B is becoming substitutional, as evidenced by HRXRD. The whole set of data suggest that after instability No 4, there are a fraction of other clusters which need a higher T to dissolve. Finally, the instability No 1 could be connected with some defects present in the lattice just after He irradiation, whose dissolution is triggered by moderate T.

4. Conclusions

In conclusion, by means of an unconventional use of HRXRD, we studied the evolution of B–B pairs formed in crystalline Si after He irradiation, revealing the main strain instabilities and the corresponding energy barriers related to the cluster dissolution mechanisms ((2–3) eV). These latter results allowed us to determine an experimental description of the B–B pair dissolution path in good agreement with *ab initio* theoretical predictions.

Acknowledgments

The authors wish to acknowledge A Sambo (Padova University) and S Tatì and C Percolla (MATIS CNR-INFM, Catania) for technical expertise.

References

[1] Jain S C, Schoenmaker W, Lindsay R, Stolk P A, Decoutere S, Willander M and Maes H E 2002 *J. Appl. Phys.* **91** 8919 and references therein
[2] Boninelli S, Mirabella S, Bruno E, Priolo F, Cristiano F, Claverie A, De Salvador D, Bisognin G and Napolitani E 2007 *Appl. Phys. Lett.* **91** 31905
[3] Cristiano F, Hebras X, Cherkashin N, Claverie A, Lerch W and Paul S 2003 *Appl. Phys. Lett.* **83** 5407
[4] De Salvador D, Napolitani E, Bisognin G, Carnera A, Bruno E, Mirabella S, Impellizzeri G and Priolo F 2005 *Appl. Phys. Lett.* **87** 221902 and references therein
[5] Solmi S, Mancini L, Milita S, Servidori M, Mannino G and Bersani M 2001 *Appl. Phys. Lett.* **79** 1103
[6] Liu X-Y, Windl W and Masquelier M P 2000 *Appl. Phys. Lett.* **77** 2018
[7] Lenoski T J, Sadigh B, Theiss S K, Caturla M-J and de la Rubia T D 2000 *Appl. Phys. Lett.* **77** 1834
[8] Windl W, Liu X-Y and Masquelier M P 2001 *Phys. Status Solidi* b **226** 37–45
[9] Cogoni M, Mattoni A, Uberuaga B P, Voter A F and Colombo L 2005 *Appl. Phys. Lett.* **87** 191912
[10] Pelaz L, Gilmer G H, Gossmann H-J, Rafferty C S, Jaraìz M and Barbolla J 1999 *Appl. Phys. Lett.* **74** 3657
[11] Piro A M, Romano L, Mirabella S and Grimaldi M G 2005 *Appl. Phys. Lett.* **86** 081906
[12] Romano L, Piro A M, Mirabella S, Grimaldi M G and Rimini E 2005 *Appl. Phys. Lett.* **87** 201905 and references therein
[13] Romano L, Piro A M, Mirabella S and Grimaldi M G 2007 *Nucl. Instrum. Methods* B **257** 146–51
[14] Romano L, Piro A M, Grimaldi M G and Rimini E 2006 *Nucl. Instrum. Methods* B **249** 181–4
[15] Bisognin G, De Salvador D, Napolitani E, Berti M, Polimeni A, Capizzi M, Rubini S, Martelli F and Franciosi A 2008 *J. Appl. Crystallogr.* **41** 366–72
[16] Raineri V, Saggio M and Rimini E 2000 *J. Mater. Res.* **15** 1449
[17] Bisognin G, De Salvador D, Napolitani E, Carnera A, Romano L, Piro A M, Mirabella S and Grimaldi M G 2006 *Nucl. Instrum. Methods* B **253** 55–8
[18] Sadigh B, Lenosky T J, Theiss S K, Caturla M-J, Diaz de la Rubia T and Foad M A 1999 *Phys. Rev. Lett.* **83** 4341
[19] Napolitani E, De Salvador D, Storti R, Carnera A, Mirabella S and Priolo F 2004 *Phys. Rev. Lett.* **93** 055901
[20] Zhu J, Diaz de la Rubia T, Yang L H, Mailhiot C and Gilmer G H 1996 *Phys. Rev.* B **54** 4741
[21] Alippi P, Colombo L, Ruggerone P, Sieck A, Seifert G and Frauenheim T 2001 *Phys. Rev.* B **64** 075207
[22] Pichler P 2004 *Intrinsic Point Defects, Impurities, and Their Diffusion in Silicon* ed S Selberherr (Berlin: Springer)
[23] Bisognin G, De Salvador D, Napolitani E, Berti M, Carnera A, Mirabella S, Romano L, Grimaldi M G and Priolo F 2007 *J. Appl. Phys.* **101** 93523
[24] Corni F, Calzolai G, Frabboni S, Nobili C, Ottaviani G, Tonini R, Cerofolini G F, Leone D, Servidori M, Brusa R S, Karwasz G P, Tiengo N and Zecca A 1999 *J. Appl. Phys.* **85** 1401
[25] Bisognin G, De Salvador D, Napolitani E, Carnera A, Bruno E, Mirabella S, Priolo F and Mattoni A 2006 *Semicond. Sci. Technol.* **21** L41–4
[26] Christensen J S, Radamson H H, Kuznetsov A Yu and Svensson B G 2003 *Appl. Phys. Lett.* **82** 2254 and references therein